OPTICA

Laser cooling a membrane-in-the-middle system close to the quantum ground state from room temperature

Sampo A. Saarinen,[1,2,†] Nenad Kralj,[1,2,3,†] Eric C. Langman,[1,2] Yeghishe Tsaturyan,[1,2,4] and Albert Schliesser[1,2,*]

[1]Niels Bohr Institute, University of Copenhagen, Blegdamsvej 17, 2100, Copenhagen, Denmark
[2]Center for Hybrid Quantum Networks, Niels Bohr Institute, University of Copenhagen, Blegdamsvej 17, 2100, Copenhagen, Denmark
[3]Institute for Gravitational Physics, Leibniz Universität Hannover, Callinstraße 38, 30167 Hannover, Germany
[4]Current address: Pritzker School of Molecular Engineering, University of Chicago, 5640 South Ellis Avenue, Chicago, Illinois 60637, USA
*albert.schliesser@nbi.ku.dk

Received 22 June 2022; revised 20 December 2022; accepted 20 January 2023; published 3 March 2023

Many protocols in quantum science and technology require initializing a system in a pure quantum state. In the context of the motional state of massive resonators, this enables studying fundamental physics at the elusive quantum–classical transition, and measuring force and acceleration with enhanced sensitivity. Laser cooling has been a method of choice to prepare mechanical resonators in the quantum ground state, one of the simplest pure states. However, to overcome the heating and decoherence by the thermal bath, this usually has to be combined with cryogenic cooling. Here, we laser-cool an ultracoherent, soft-clamped mechanical resonator close to the quantum ground state directly from room temperature. To this end, we implement the versatile membrane-in-the-middle setup with one fiber mirror and one phononic crystal mirror, which reaches a quantum cooperativity close to unity already at room temperature. We furthermore introduce a powerful combination of coherent and measurement-based quantum control techniques, which allows us to mitigate thermal intermodulation noise. The lowest occupancy we reach is 30 phonons, limited by measurement imprecision. Doing away with the necessity for cryogenic cooling should further facilitate the spread of optomechanical quantum technologies.

https://doi.org/10.1364/OPTICA.468590

1. INTRODUCTION

Over the last decade, the relative simplicity and great versatility of membrane-in-the-middle (MIM) systems [1] have rendered them a highly popular choice for a variety of optomechanics experiments. To name just a few examples, they have been used for early demonstrations of optomechanical effects such as dynamical [2–5] and quantum backaction [6], optomechanically induced transparency [7], and Raman ratio thermometry [8,9], to implement coupling between mechanical and atomic degrees of freedom [10–13], to explore novel routes for enhanced sensitivity in gravitational wave detection [14–16], to study multimode [17–19] and topological physics [20], to manipulate the quantum state of light [21,22], and to realize electro–opto–mechanical transducers [23–26]. More recently, force sensing [27–29] and imaging [30] applications have received particular attention, due to the very low thermomechanical force noise [31–33], and the potential for very efficient optical detection of the sensor state [34,35]. Indeed, using a broadband correlation technique [36,37], this platform has even allowed continuous force measurements beyond the standard quantum limit (SQL) for the first time [38].

However, to reach the quantum regime, it has so far been necessary to cool the membrane to cryogenic temperatures [6,8–11,13,18,21,22,24–26,34,35,38]. For even greater flexibility and versatility, it would be desirable to be able to operate in the quantum regime already at room temperature. To date, few mechanical systems have even approached the quantum regime at room temperature, including optically levitated nanoparticles [39,40], select nano- [41–43] and micromechanical devices [44], as well as a set of macroscopic mirrors in a gravitational wave observatory [45]. Save for the latter, a broad range of applications have yet to be demonstrated with these platforms, in contrast to MIM systems. Our goal is therefore to implement a room-temperature MIM system in the quantum regime.

A key enabler towards this goal is a recently developed ultracoherent mechanical system, a "soft-clamped" membrane resonator [33], whose coherence *at room temperature* rivals those of standard membranes at cryogenic temperatures [6,18]. We also bring to bear several techniques to mitigate background thermal noises in the system, including a phononic mirror and a combination of sideband cooling and feedback cooling.

Corrected 06 March 2023

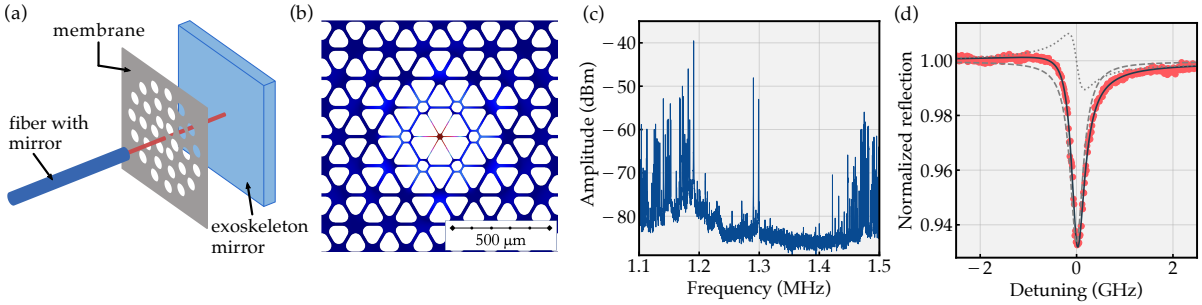

Fig. 1. (a) Sketch of the cavity assembly with main components. (b) Top view of membrane geometry, with a central defect in a phononic crystal. Color code indicates simulated out-of-plane displacement (increasing from blue to red shades). (c) Thermal spectrum of the Dandelion, as measured inside the fiber cavity. It features a bandgap in the region from 1.2 MHz to 1.5 MHz and two soft-clamped defect modes around its center. (d) Cavity resonance as measured in reflection. The asymmetric line shape is a consequence of the filtering done by the fiber mode. The fit to the model (solid black line) can be decomposed into the Lorentzian and dispersive contributions (dashed and dotted light gray lines, respectively).

2. SOFT-CLAMPED MEMBRANE-IN-THE-MIDDLE SYSTEM

The membrane is placed inside a Fabry–Pérot optical resonator (Fig. 1), between a node and an anti-node of the standing optical wave in the cavity. We thereby implement the standard MIM dispersive optomechanical coupling [1] described by the Hamiltonian [46,47] $H_{\rm om} = \hbar g_0 a^\dagger a (b + b^\dagger)$. Here, $\hbar$ is the reduced Planck constant, g_0 the vacuum optomechanical coupling rate, and $a\,(a^\dagger)$ and $b\,(b^\dagger)$ the optical and mechanical annihilation (creation) operators, respectively. The membrane is 15 nm thick and patterned with a phononic crystal, which affords soft-clamping of an out-of-plane mechanical mode localized close to an intentionally introduced crystal defect [33]. In this work, we introduce a new design for both the crystal and the defect (which we refer to as the "Dandelion" design); see Fig. 1(b). Compared to the design used in our previous works [13,22,29,33–35,38], Dandelion-class defects exhibit significantly lower masses (up to a 30-fold reduction) when fabricated from identical substrates and targeting the same frequency and Q-factors. Additionally, the mechanical mode can be centered in an ∼50% bigger bandgap, with typically only one extra mechanical mode in the bandgap (two total). However, these benefits come with a significant reduction in the size of the pad at the defect center, which can lead to complications with large cavity waists and/or optical alignment. As such, the optimal for any application is not necessarily the design with the smallest mass, highest Q-factor, or other figure of merit.

Specifically due to alignment tolerances, the particular design used in this work is a medium-size Dandelion with a central pad approximately 30 μm across, resulting in a mechanical mode with resonance frequency $\Omega_{\rm m}/2\pi = 1.3$ MHz and modal mass $m_{\rm eff} \approx 200$ pg. This results in a relatively large amplitude of zero-point fluctuations, $x_{\rm zpf} = \sqrt{\hbar/2m_{\rm eff}\Omega_{\rm m}} = 5.7$ fm. Due to the soft-clamping effect, we achieve intrinsic damping rates $\Gamma_{\rm m}/2\pi \approx 9$ mHz, corresponding to quality factors as high as $Q_{\rm m} = \Omega_{\rm m}/\Gamma_{\rm m} = 1.4 \times 10^8$ with these devices at room temperature, $T \approx 300$ K, where the occupation of the mechanical bath is as high as $\bar{n}_{\rm th} \approx k_{\rm B} T/\hbar\Omega_{\rm m} \approx 5.1 \cdot 10^6$ ($k_{\rm B}$ is the Boltzmann constant). This implies a thermomechanical decoherence rate of $\gamma = \bar{n}_{\rm th}\Gamma_{\rm m} \approx 2\pi \cdot 48$ kHz. In turn, this corresponds to $\Omega_{\rm m}/\gamma \approx 27$ coherent oscillations, comparing favorably to similar experiments (four coherent oscillations [41]) and even levitated optomechanical systems (≲15 coherent oscillations [39]).

The cavity consists of one curved and one flat mirror. We fabricate the curved mirror by laser-machining a concave indentation into the facet of a single-mode fiber, and subsequently coating it with a high-reflectivity coating [48,49]. To realize the flat mirror, a slightly different coating is deposited on a flat Pyrex glass wafer that has been bonded to a silicon "exoskeleton" support structure, whose role will be detailed in Section 4.B. The mirrors are set up to face each other with a distance of $L \approx 95$ μm. Details on the fabrication of the mirrors and the mechanical setup are provided in Supplement 1.

The mirror coatings are designed to provide a one-sided, high-finesse cavity at a wavelength of around 1550 nm. Independent measurements of the actually realized mirrors' power transmissivities, T_f and T_e for the fiber and exoskeleton mirror, respectively, suggest an overcoupling of $\eta_{\rm c} = T_f/(T_f + T_e) \approx 0.9$ for the cavity coupled through the fiber mirror. For the assembled cavity including a membrane, we measure the reflection signal through the (more transmissive) fiber mirror, as shown in Fig. 1(d). Using the model in [50] to fit the data, we obtain a FWHM cavity linewidth of $\kappa/2\pi = 340$ MHz, corresponding to a finesse of $\mathcal{F} \approx 4400$. Note that the spatial filtering of the cavity leakage by the fiber mode leads to an asymmetric reflection signature (with two contributions of Lorentzian and dispersive shapes), the depth of which is not limited by the mode-matching efficiency ε between the cavity and detected optical modes. See Supplement 1 for more details on the model.

The geometry of the indentation in the fiber mirror is approximately spherical with a 300 μm radius of curvature, leading to an approximately 10 μm waist of the cavity's fundamental optical mode. This allows good transverse overlap ($\xi \sim 1$) of the optical and mechanical mode shapes, even for the small—and therefore low-mass—defect of the Dandelion design. Together with the short cavity length, this facilitates large vacuum optomechanical coupling, which can, for the optimal position of the membrane within the cavity standing wave, be approximated as

$$g_0^{\rm max} \approx 2\frac{\omega_{\rm c}}{L}|r|x_{\rm zpf}\xi, \tag{1}$$

where $\omega_{\rm c}$ is the cavity resonance frequency, and r is the membrane's optical (field) reflectivity. Indeed, for the parameters of the system, we expect a coupling rate of $g_0/2\pi \lesssim 3.3$ kHz.

3. DYNAMICAL BACKACTION

Broadly speaking, to reach the quantum regime, it is necessary to achieve a quantum cooperativity $C_q = 4g^2/(\kappa\gamma) \gtrsim 1$, where κ and γ are the optical and mechanical decoherence rates, respectively, and $g = g_0\sqrt{\bar{n}_{cav}}$ is the field-enhanced coupling rate with the intracavity photon number $\bar{n}_{cav}$. In a first set of experiments, we infer the obtained coupling by analyzing dynamical backaction [2–5] on the mechanical mode.

To this end, we couple a low-noise laser (NKT Photonics Koheras Basik E15) of wavelength $\lambda \approx 1542$ nm to the cavity. We derive two beams from this laser: a "probe" beam to lock the cavity on resonance with one of its fundamental modes using a Pound–Drever–Hall locking scheme, and to read out the mechanical motion via a homodyne interferometer. A second, "cooling" beam is offset by −80 MHz via a fiber-based acousto-optic modulator, and its polarization is made orthogonal to that of the probe. These two facts help minimize the unwanted effect of the cooling beam on the measurement record. Figure 2(a) shows the schematic of the experimental setup, an extended discussion of which is presented in Supplement 1.

As we increase the cooling beam power, we observe the evolution of the mechanical noise spectrum through the probe homodyne detector. We extract the mechanical frequency shift $\delta\Omega_m^c$ resulting from the optical spring effect, as a function of the cooling beam power (cf. Fig. 2(b)). The standard model for the mechanical frequency shift by an optical spring [46],

$$\delta\Omega_m^c = g_c^2\left(\frac{\Delta_c - \Omega_m}{\kappa^2/4 + (\Delta_c - \Omega_m)^2} + \frac{\Delta_c + \Omega_m}{\kappa^2/4 + (\Delta_c + \Omega_m)^2}\right), \tag{2}$$

supplied with the independently known Ω_m, κ, and detuning Δ_c, allows us to extract the field-enhanced coupling rate g_c as a function of measured power. The index "c" here refers to the cooling beam. For a given power, we can estimate the intracavity photon number by estimating the incoupling efficiency of light. In this manner, we infer an experimental value for the vacuum optomechanical coupling rate of $g_0/2\pi = 2.3$ kHz, in good agreement with the theoretical value, assuming slightly sub-optimal longitudinal and transverse positioning of the membrane.

We also compare the observed broadening of the mechanical linewidth with the expected damping due to dynamical backaction of the cooling beam [46],

$$\Gamma_m^c = g_c^2\left(\frac{\kappa}{\kappa^2/4 + (\Delta_c + \Omega_m)^2} - \frac{\kappa}{\kappa^2/4 + (\Delta_c - \Omega_m)^2}\right), \tag{3}$$

for all of the inferred couplings g_c, and find good agreement. Specifically, in Fig. 2(c), we show the total damping rate $\Gamma_m^{tot} = \Gamma_m + \Gamma_m^p + \Gamma_m^c$, with Γ_m^p the contribution from optical damping by the (very slightly red-detuned) probe beam. To allow for this probe-induced damping, the dashed line is a fit with the vertical offset as the only free parameter, but is otherwise fully constrained by independently known parameters (Ω_m, κ, and Δ_c) and the fit of the optical spring. The fit to the linewidths yields $\Gamma_m^p/2\pi = 4.6$ Hz, corresponding to a probe detuning $\Delta_p/2\pi \lesssim -2$ MHz. The zero-power linewidth is likely overestimated due to inhomogeneous broadening caused by a fluctuation in coupled laser power.

Finally, we confirm that we can increase the probe power further, into a regime where $C_q \approx 1$ would be expected, without the onset of optomechanical (or other) instabilities.

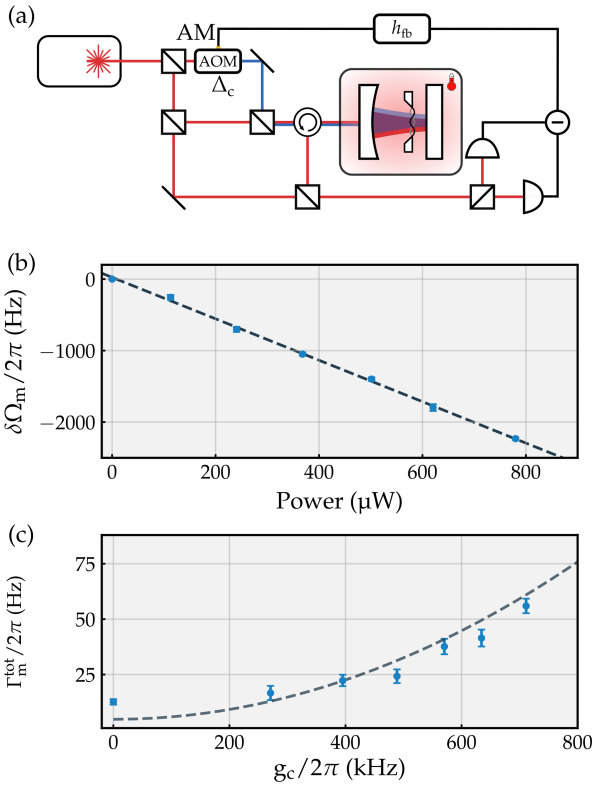

Fig. 2. (a) Schematic of the experimental setup. The probe (red) and cooling (blue) beams are derived from a single laser. The probe is locked on resonance with the cavity and used for a homodyne readout of the membrane motion. The feedback force is exerted by convolving this measurement with a filter function h_{fb} and using it to modulate the amplitude of the cooling beam. The cooling beam is detuned from the cavity by $\Delta_c/2\pi = -80$ MHz and thus also provides sideband cooling. The optomechanical cavity is kept in a vacuum chamber at a pressure $p_{UHV} \approx 2 \times 10^{-8}$ mbar. (b) Mechanical frequency shift due to the cooling beam as a function of input optical power. The dashed line is a linear fit to the data following Eq. (2), with $g_c^2 \propto$ (Power). (c) Optically broadened mechanical linewidth as a function of the cooling beam coupling rate g_c. With g_c extracted from the measured power based on the fit in (b), the only fit parameter for the dashed line is a vertical offset due to a small cooling by the probe. The data points in both (b) and (c) are mean values over five acquisitions, and the error bars correspond to the standard errors of the mean.

4. LASER COOLING CLOSE TO THE QUANTUM GROUND STATE

A. Theoretical Cooling Limits

Next we aim at preparing the mechanical system in a pure quantum state—specifically, the quantum ground state. That is, starting from the equilibrium value $\bar{n}_{th} = 5.1 \cdot 10^6$, we want to reduce the residual mechanical occupation $\bar{n} = \langle b^\dagger b\rangle \to 0$. Laser sideband cooling has been used with great success to cool mechanical oscillators, including MIM systems [2–5,18,38]. Adapting the theory of sideband cooling yields the final occupation [46]

$$\bar{n} = \frac{\bar{n}_{th}\Gamma_m(1 + C_q) + \bar{n}_m^c\Gamma_m^c}{\Gamma_m^{tot}}, \tag{4}$$

where Γ_m^{tot} in the denominator allows for a small probe detuning, the numerator accounts for the probe's quantum backaction (with $C_q \lesssim 1$ the probe's quantum cooperativity), and

$$\bar{n}_{\mathrm{m}}^{\mathrm{c}} = \frac{(\Omega_{\mathrm{m}} + \Delta_{\mathrm{c}})^2 + (\kappa/2)^2}{-4\Delta_{\mathrm{c}}\Omega_{\mathrm{m}}} \tag{5}$$

is the minimum occupancy that can be reached in the limit of strong cooling $\Gamma_{\mathrm{m}}^{\mathrm{c}} \gg \bar{n}_{\mathrm{th}}\Gamma_{\mathrm{m}}(1 + C_{\mathrm{q}})$, due to quantum backaction of the cooling beam. In the unresolved-sideband regime with $\kappa \gg \Omega_{\mathrm{m}}$, in which we work here, $\bar{n}_{\mathrm{m}}^{\mathrm{c}} \approx \kappa/4\Omega_{\mathrm{m}}$ for optimal detuning Δ_{c}, corresponding to about 65 phonons for the parameters of our system. We note that Eq. (4) should, in principle, also contain classical backaction, i.e., photothermal heating and intensity noise heating, which would manifest as an effective thermal bath occupation that increases with optical power. The analysis of the mechanical area as a function of optical power presented in Supplement 1 shows, however, that this effect is negligible.

Given that sideband cooling to the ground state is prohibited by quantum backaction, we additionally expect to be using measurement-based quantum control techniques [34,35,40,47,51–54] to reach it. In these approaches, one tracks the mechanical position $x(t) = x_{\mathrm{zpf}}(b(t) + b^{\dagger}(t))$ through the optical signal, in our case the output $y(t)$ of the homodyne interferometer detecting the probe light. A sufficiently precise measurement record allows tracking the state of the oscillator, and preparing it in a highly pure conditional quantum state [35]. Alternatively, one can derive a feedback force $F_{\mathrm{fb}}(t) = h_{\mathrm{fb}}(t) * y(t)$ from the measured displacement, where $h_{\mathrm{fb}}(t)$ is a filter kernel, and $*$ denotes a convolution. Applying this force to the mechanical resonator allows preparing it in its ground state unconditionally [34].

Importantly, the measured signal $y(t) = x(t) + x_{\mathrm{imp}}(t)$ contains, apart from the true position $x(t)$, also the imprecision $x_{\mathrm{imp}}(t)$, a noise background inevitable in the kind of interferometric measurement discussed here [55]. For optimal gain in the feedback loop, the minimum occupation that can be reached can be written approximately as (see Supplement 1)

$$\bar{n}_{\mathrm{min}}^{\mathrm{fb}} \approx \sqrt{\frac{\bar{S}_{FF}^{\mathrm{tot}} \cdot \bar{S}_{xx}^{\mathrm{imp}}}{4\hbar^2}} - \frac{1}{2}. \tag{6}$$

Here, $\bar{S}_{FF}^{\mathrm{tot}}$ is the (symmetrized, single-sided) spectral density of force fluctuations driving the mechanical resonator, whereas $\bar{S}_{xx}^{\mathrm{imp}}$ is the spectral density of x_{imp}. We assume these spectral densities are constant in the relevant range around the mechanical frequency Ω_{m} and have dropped the frequency argument for brevity. The total force fluctuations $\bar{S}_{FF}^{\mathrm{tot}} = \bar{S}_{FF}^{\mathrm{th}} + \bar{S}_{FF}^{\mathrm{rp}}$ contain both the thermal Langevin force noise $\bar{S}_{FF}^{\mathrm{th}} = 4m_{\mathrm{eff}}\Gamma_{\mathrm{m}}k_{\mathrm{B}}T$, as well as the radiation pressure fluctuations of the intracavity light field(s) $\bar{S}_{FF}^{\mathrm{rp}}$. If the latter are given only by quantum fluctuations, we have $\bar{S}_{FF}^{\mathrm{rp}} = C_{\mathrm{q}}\bar{S}_{FF}^{\mathrm{th}}$.

The imprecision, in turn, must at least contain the quantum (shot) noise in the optical detector. This ensures that the Heisenberg measurement-disturbance uncertainty relation $\bar{S}_{FF}^{\mathrm{rp}}\bar{S}_{xx}^{\mathrm{imp}} \geq \hbar^2$ is always respected [46,47,55]. For imperfect detection efficiency $\eta_{\mathrm{det}} < 1$, the imprecision as referenced to equivalent mechanical displacement grows, and $\bar{S}_{FF}^{\mathrm{rp}}\bar{S}_{xx}^{\mathrm{imp}} = \hbar^2/\eta_{\mathrm{det}}$ if both radiation pressure and imprecision noise are limited by quantum fluctuations otherwise [56]. We can additionally take into account the classical contribution to the imprecision noise $\bar{S}_{xx}^{\mathrm{imp,cl}}$, for example, due to fluctuations of the cavity mirrors, which produce cavity length changes unrelated to (but indistinguishable from) membrane motion. We then have $\bar{S}_{xx}^{\mathrm{imp}} = \bar{S}_{xx}^{\mathrm{imp,q}} + \bar{S}_{xx}^{\mathrm{imp,cl}}$ and $\bar{S}_{xx}^{\mathrm{imp,q}} = \hbar^2/\eta_{\mathrm{det}}C_{\mathrm{q}}\bar{S}_{FF}^{\mathrm{th}}$, with which we can rewrite Eq. (6) as

$$\bar{n}_{\mathrm{min}}^{\mathrm{fb}} \approx \sqrt{(1 + C_{\mathrm{q}})\left(\frac{1}{4\eta_{\mathrm{det}}C_{\mathrm{q}}} + \frac{\bar{S}_{xx}^{\mathrm{imp,cl}} \cdot \bar{n}_{\mathrm{th}}\Gamma_{\mathrm{m}}}{2x_{\mathrm{zpf}}^2}\right)} - \frac{1}{2}. \tag{7}$$

Evidently, for quantum-limited ($\bar{S}_{xx}^{\mathrm{imp,cl}} \to 0$), strong ($C_{\mathrm{q}} \gg 1$), and efficient ($\eta_{\mathrm{det}} \to 1$) measurement, the ground state can be reached ($\bar{n}_{\mathrm{min}}^{\mathrm{fb}} \to 0$), as demonstrated in [34] for a MIM system and [40] for a levitated nanoparticle.

B. Imprecision Noise Analysis

Key challenges when moving from cryogenic to room temperature operation include that not only the quantum cooperativity $C_{\mathrm{q}} \propto 1/\bar{n}_{\mathrm{th}}$ but also the classical imprecision contribution ($\propto \bar{S}_{xx}^{\mathrm{imp,cl}} \cdot \bar{n}_{\mathrm{th}}$) in Eq. (7) need to be compatible with a ∼100-fold increase of $\bar{n}_{\mathrm{th}}$, given that most cryogenic experiments operate at ∼4 K or even lower. Several contributions must be considered here.

The first is laser frequency (or phase) noise. The spectral density of laser frequency fluctuations $\bar{S}_{\omega\omega}$ close to Ω_{m} can be rescaled to effective displacement using the frequency pull parameter $\mathrm{d}\omega_{\mathrm{c}}/\mathrm{d}x = g_0/x_{\mathrm{zpf}}$ [cf. Eq. (1)]. If the corresponding imprecision $\bar{S}_{xx}^{\mathrm{imp,ln}} = \bar{S}_{\omega\omega}/(\mathrm{d}\omega_{\mathrm{c}}/\mathrm{d}x)^2$ dominates the quantum imprecision, this leads to a minimum occupation of the order of $(\bar{S}_{\omega\omega} \cdot \bar{n}_{\mathrm{th}}\Gamma_{\mathrm{m}}/g_0^2)^{1/2}$ for $C_{\mathrm{q}} \approx 1$. Interestingly, a similar limit has been derived and observed for laser sideband cooling [57–59]. In our experiment, the frequency noise of the employed laser is specified as $\bar{S}_{\omega\omega} \lesssim (2\pi \cdot 1\ \mathrm{Hz})^2/\mathrm{Hz}$ [60], leading to a negligible contribution as $\bar{S}_{\omega\omega} \cdot \bar{n}_{\mathrm{th}}\Gamma_{\mathrm{m}}/2g_0^2 \approx 0.03$, much smaller than the quantum imprecision term $1/4\eta_{\mathrm{det}}C_{\mathrm{q}}$ (see below).

To analyze the second potential contribution, we need to note that the transduction of the cavity frequency fluctuations into the optical field is inherently nonlinear. As shown in [61], these nonlinearly transduced frequency fluctuations result in a broadband "thermal intermodulation noise" (TIN) that can dominate the noise in photodetection when the linearly transduced fluctuations are small, e.g., when detecting the intensity of a resonant beam (as in [61]). Conversely, for a homodyne measurement of a resonant beam's phase, employed in our work, the linear contribution is maximal. Moreover, the leading nonlinear term is not quadratic, but cubic in small fluctuations, which leads to a more favorable scaling of different contributions to TIN (see Supplement 1 for more details). Finally, because our MIM cavity is deep in the unresolved-sideband regime, the cooling beam provides sideband cooling of a wide range of mechanical modes, which should alleviate the effect of TIN even further [62], such that we expect not to be limited by it. While TIN-related intensity noise can still be present in the system, it neither appears in the cavity scans [Fig. 1(d)] nor does it manifest as excess heating, as discussed before.

A third relevant source of classical imprecision noise is thermal fluctuations in the cavity mirrors. This phenomenon has been studied extremely carefully in the context of the large mirrors employed in gravitational wave observatories, and a number of possible mechanisms have been identified [63]. More compact cavities with millimeter-scale mirrors are typically dominated by the thermal fluctuations of the mirror substrate, displacing the boundary off which the light is reflected. Since the mirror substrates in general support a discrete set of mechanical resonance

modes, the spectra of these fluctuations are expected to consist of a series of relatively sharp peaks, depending on the Q-factor of the mirror modes. Such spectra have been systematically studied for some two decades [64–66], and indeed even used as mechanical modes in early optomechanics experiments [64]. They have also constituted a limiting factor of MIM experiments, where they can mask quantum effects in the spectral regions where the peaks appear [18,38,67]. At room temperature, peak displacement spectral densities at the level of $(1-10\ \mathrm{am})^2/\mathrm{Hz}$ have been measured for commonly employed mirror geometries [64–66].

The purpose of our flat mirror's "exoskeleton" [shown in Fig. 3(a)] is to reduce the impact of this noise. Indeed, this silicon substrate is structured with a phononic crystal similar to the one employed as membrane support in earlier work [68,69]. It is modified in such a way that if bonded to the Pyrex wafer that carries the mirror reflective coating, the joint structure exhibits an acoustic bandgap in the MHz frequency regime. We have verified the existence of the bandgap by measuring the out-of-plane motion of the mirror surface in response to a swept excitation with a piezoelectric transducer [Fig. 3(b)]. Within the bandgap, we therefore expect no substrate thermal noise peaks to appear at a relevant level.

Informed by earlier studies of guided acoustic-wave Brillouin scattering in single-mode fiber [70], we would expect the acoustic resonances of the fiber mirror to exhibit a sparse spectrum and in particular remain confined to high frequencies $\gtrsim 10$ MHz. A dedicated study [71] of a fiber cavity has revealed, however, that, e.g., fiber bending modes can occur already in the MHz regime, and more importantly, also the existence of a broadband noise at the level of about $(20\ \mathrm{am})^2/\mathrm{Hz}$ in the MHz frequency region.

We have independently analyzed the background noise in our composite exoskeleton/fiber-mirror cavity, with a dedicated measurement of its apparent displacement noise with the membrane removed. The result is shown in Fig. 3(c). Not only does it display peaks already above 2 MHz, but it does indeed also show broadband noise, which reaches the level of $\sim(10\ \mathrm{am})^2/\mathrm{Hz}$ at 1 MHz, well compatible with earlier measurements [71] (note that we use only one fiber mirror). We interpret the absence of any signature of the exoskeleton's bandgap in this joint noise spectrum to be a consequence of the fact that the latter is dominated by broadband noise of the fiber mirror. Whereas this noise is certainly sub-ideal, we can tolerate the associated level of classical imprecision (with $\bar{S}_{xx}^{\mathrm{imp,cl}} \cdot \bar{n}_{\mathrm{th}}\Gamma_{\mathrm{m}}/2x_{\mathrm{zpf}}^2 \approx 0.5$) in the current experiments, since the quantum noise contribution is much larger (see below).

Quantum noise in the detection is the last contribution to consider. For a resonant probe in the unresolved-sideband regime, the equivalent displacement noise power spectral density is given by $\bar{S}_{xx}^{\mathrm{imp,q}} = \hbar^2/\eta_{\mathrm{det}}C_{\mathrm{q}}\bar{S}_{FF}^{\mathrm{th}} = x_{\mathrm{zpf}}^2/2\eta_{\mathrm{det}}C_{\mathrm{q}}\gamma$. Here, the overall detection efficiency is determined by the product $\eta_{\mathrm{det}} = \varepsilon \cdot \eta_{\mathrm{c}} \cdot |\beta| \cdot \mathcal{V} \cdot P_{\mathrm{QE}}$, with the efficiency $\varepsilon \cdot \eta_{\mathrm{c}}$ for coupling cavity photons into the guided fiber mode, fiber losses $|\beta|$, homodyne fringe visibility $\mathcal{V}$, and the photodetectors' quantum efficiency P_{QE}. We achieve $\eta_{\mathrm{det}} \approx 1.2\%$, dominated by a relatively low cavity mode matching $\varepsilon \approx 4\%$; see Supplement 1 for details. We determine the quantum cooperativity $C_{\mathrm{q}} = 4g^2/\kappa\gamma$ of the probe from the measured power ratio of the two beams, their known detunings, and the cooling beam's coupling rate g_{c} as determined by the dynamical backaction measurements described in Section 3.

Our laser does not provide enough optical power to reach unity cooperativity with the probe, and simultaneously feed the cooling beam and local oscillator with sufficient power. We therefore operate with a relatively modest probe power, corresponding to $C_{\mathrm{q}} = 0.1$. We then have enough optical power available for the local oscillator to overwhelm the detectors' electronic noise with shot noise. Whereas higher quantum cooperativity would certainly be desirable, the achieved value constitutes a significant advancement over many tabletop room-temperature experiments, reaching $C_{\mathrm{q}} \approx 10^{-5}$ [43], $C_{\mathrm{q}} < 10^{-4}$ [5], $C_{\mathrm{q}} \approx 4 \cdot 10^{-3}$ [41], and $C_{\mathrm{q}} \approx 5 \cdot 10^{-3}$ [42], and is on par with that in [44]. With this available probe power, the expected quantum imprecision of $\bar{S}_{xx}^{\mathrm{imp,q}} \approx (210\ \mathrm{am})^2/\mathrm{Hz}$ is still well above the mirror noise.

C. Cooling Results

To cool the membrane mode close to its motional ground state, we employ the setup shown in Fig. 2(a), and described already in Section 3. Additional details can be found in Supplement 1. Cooling proceeds via the combined effect of laser sideband and feedback cooling. That is, the cooling beam is detuned by $\Delta_{\mathrm{c}}/2\pi \approx -80$ MHz from the cavity resonance, and its dynamical backaction damps the mechanical motion. The corresponding "anchor" spectrum of mechanical fluctuations is recorded by homodyne detection of the second, probe beam. The broadened mechanical resonance width $\Gamma_{\mathrm{m}}^{\mathrm{tot}}/2\pi \approx 52$ Hz can be straightforwardly extracted from the homodyne spectrum via a Lorentzian fit. Together with independently determined optical $(\Delta_{\mathrm{c}}, \kappa)$ and mechanical $(\Omega_{\mathrm{m}}, \Gamma_{\mathrm{m}})$ parameters, we can estimate the resulting occupation $\bar{n}$ of the mode after sideband cooling from Eqs. (4) and (5). Here, the bare mechanical damping Γ_{m} is obtained from ringdown measurements in a different setup and corrected for slightly different pressure; see Supplement 1 for details. The calculated sideband-cooled mode occupation $\bar{n} \approx 1070$ quanta is then used to calibrate the homodyne spectrum, which is originally recorded in electrical (voltage) units. That is, the measured homodyne spectrum $\bar{S}_{yy}(\Omega) = \bar{S}_{xx}(\Omega) + \bar{S}_{xx}^{\mathrm{imp}}$ is calibrated in displacement units so that

$$\bar{n} = \int_0^\infty \frac{\bar{S}_{xx}(\Omega)}{2x_{\mathrm{zpf}}^2}\frac{\mathrm{d}\Omega}{2\pi} - \frac{1}{2} \tag{8}$$

holds, whereby $\bar{S}_{xx}(\Omega) = |\chi_{\mathrm{m}}^{\mathrm{tot}}(\Omega)|^2\bar{S}_{FF}^{\mathrm{tot}}$, and $\chi_{\mathrm{m}}^{\mathrm{tot}}(\Omega)$ is the Lorentzian mechanical susceptibility modified by dynamical backaction.

We now turn on the feedback cooling of the membrane mode. To this end, the homodyne signal $y(t)$ is filtered and amplified, and subsequently used to modulate the radiation-pressure force $F_{\mathrm{fb}}(t) = h_{\mathrm{fb}}(t) * y(t)$ exerted by the cooling beam via the acousto-optic modulator [Fig. 2(a)]. In the frequency domain, the filter's transfer function is of the form $h_{\mathrm{fb}}(\Omega) = h_{\mathrm{main}}(\Omega) + h_{\mathrm{aux}}(\Omega)$, with

$$h_{\mathrm{main}}(\Omega) = G_{\mathrm{fb}}e^{i(\Omega\tau_{\mathrm{fb}}-\phi_{\mathrm{fb}})}\left[\frac{\Gamma_{\mathrm{fb}}\Omega}{\Omega_{\mathrm{fb}}^2 - \Omega^2 - i\Gamma_{\mathrm{fb}}\Omega}\right]^2. \tag{9}$$

Here, G_{fb} is the overall feedback gain, the main filter central frequency is $\Omega_{\mathrm{fb}}/2\pi = 1.34$ MHz, and the bandwidth $\Gamma_{\mathrm{fb}}/2\pi = 77.86$ kHz. The total delay is measured to be $\tau_{\mathrm{fb}} \approx 300$ ns, and the phase ϕ_{fb} is adjusted so as to give $\arg(h_{\mathrm{fb}}(\Omega_{\mathrm{m}}^{\mathrm{tot}})) \approx \pi/2$ (where $\Omega_{\mathrm{m}}^{\mathrm{tot}} = \Omega_{\mathrm{m}} + \delta\Omega_{\mathrm{m}}^{\mathrm{p}} + \delta\Omega_{\mathrm{m}}^{\mathrm{c}}$, and $\delta\Omega_{\mathrm{m}}^{\mathrm{p}}$ is the optical spring from

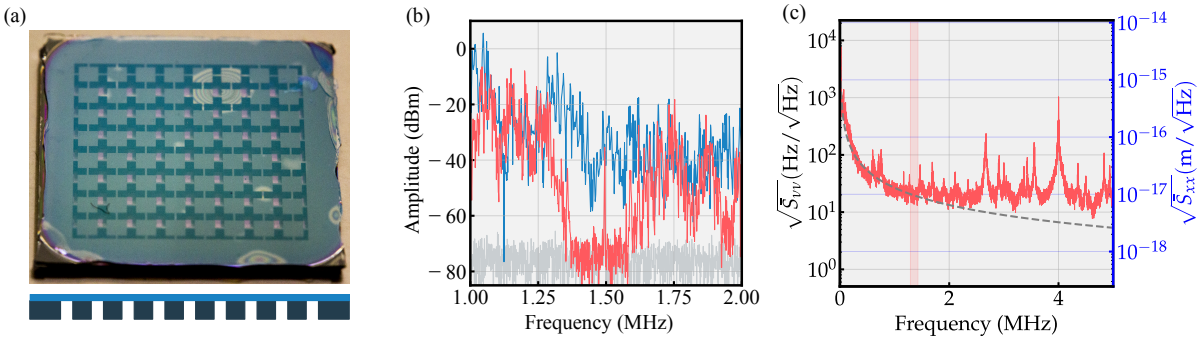

Fig. 3. (a) Photograph of an exoskeleton mirror, showing the silicon phononic crystal structure underneath the Pyrex wafer, on which a mirror was coated. Interference fringes indicate areas where the Pyrex–silicon bonding was not successful. Below is a schematic cross section of the device. (b) Spectrum of the driven response on different parts of the exoskeleton mirror: the center (red) exhibits a suppression compared to the frame (blue) for frequencies in a window around 1.5 MHz. The sharp peak within this window is an externally applied calibration tone. The light gray trace corresponds to detection noise. (c) Measured homodyne spectrum of the empty optical cavity, presented as frequency noise (left axis, black) and displacement noise (right axis, blue). The dashed gray line indicates (frequency)$^{-1}$ scaling. Both this behavior at low frequencies and the discernible peaks have been observed in fiber cavities. The light red shading indicates the frequency region of the exoskeleton bandgap.

the probe), which corresponds to $F_{\rm fb}$ approximating a friction force on the membrane. The function $h_{\rm aux}(\Omega)$ represents a narrow auxiliary filter designed to stabilize a mechanical mode just outside of the bandgap, excited by the main filter, while maintaining $h_{\rm fb}(\Omega_{\rm m}^{\rm tot}) \approx h_{\rm main}(\Omega_{\rm m}^{\rm tot})$. More information on the filter and its implementation can be found in Supplement 1.

Closing the feedback loop leads to a modified susceptibility of the mechanical mode to forces:

$$\chi_{\rm fb}(\Omega) = \frac{\chi_{\rm m}^{\rm tot}(\Omega)}{1 - \chi_{\rm m}^{\rm tot}(\Omega) h_{\rm fb}(\Omega)}. \tag{10}$$

Furthermore, also the measurement (imprecision) noise is now fed back as a force, so that

$$\bar{S}_{xx}(\Omega) = |\chi_{\rm fb}(\Omega)|^2 \left(\bar{S}_{FF}^{\rm tot} + |h_{\rm fb}(\Omega)|^2 \bar{S}_{xx}^{\rm imp}\right), \tag{11}$$

whereas the measured (in-loop) homodyne spectra are modified as

$$\bar{S}_{yy}(\Omega) = |\chi_{\rm fb}(\Omega)|^2 \left(\bar{S}_{FF}^{\rm tot} + |\chi_{\rm m}^{\rm tot}(\Omega)|^{-2} \bar{S}_{xx}^{\rm imp}\right). \tag{12}$$

Figure 4 shows the homodyne spectra measured with the feedback loop closed, and plotted normalized to the peak spectral density in the ground state $\bar{S}_{\rm xzp} \equiv 4x_{\rm zpf}^2/\Gamma_{\rm m}$. Here, we use the same conversion factor for the homodyne spectra from electrical (voltage) to displacement units as obtained for the only sideband-cooled, anchor spectrum described above, under the reasonable assumption that this conversion is not affected by changes in the feedback gain.

We fit the model of Eq. (12) to these spectra, adjusting the free parameters $G_{\rm fb}$, $\phi_{\rm fb}$ and the measurement imprecision in units of quanta, $\bar{n}_{\rm imp} = \bar{S}_{xx}^{\rm imp}/(2\bar{S}_{\rm xzp})$. The total force noise in units of quanta, $\bar{n}_{\rm tot} = \bar{S}_{FF}^{\rm tot}\bar{S}_{\rm xzp}/(8\hbar^2)$, is fixed to the value expected from the sum of thermal bath and quantum backaction heating. Other parameters of the model are extracted from the homodyne spectrum in the absence of feedback ($\Omega_{\rm m}^{\rm tot}$, $\Gamma_{\rm m}^{\rm tot}$) or measured independently. The best-fit values of the fitted parameters as a function of gain are shown in Supplement 1. We plug these best-fit values into Eq. (11), and integrate the resulting displacement spectral density, as in Eq. (8), to obtain the mechanical occupation $\bar{n}$ equivalent to the measured spectra. The results are shown in Fig. 4(b) as a function of feedback gain. As a sanity check, the described analysis is done also for the anchor spectrum, constraining $G_{\rm fb} \approx 0$, and the estimated sideband-cooled occupancy is obtained to within $\approx 1\%$.

The lowest occupancy we have obtained is $\bar{n} = 30 \pm 8$, where the confidence interval is derived by propagating the statistical uncertainty in the area of the anchor spectrum, which is used for calibrating the feedback-cooled spectra. The uncertainty propagated from those of the fit parameters for the feedback-cooled spectrum is negligible in comparison. We also expect systematic effects such as power or polarization drifts to not contribute significant additional uncertainty. From fits to the calibrated spectra, we extract a very low number of imprecision noise quanta, with the average over all gain values being $\bar{n}_{\rm imp} = (3.2 \pm 0.6) \times 10^{-5}$, corresponding to $\bar{S}_{xx}^{\rm imp} = (370 \pm 20\ {\rm am})^2/{\rm Hz}$. Still, this number is above the expected quantum imprecision noise. Correspondingly, for higher gains, the achieved occupation reaches the limit of 30 quanta expected from integrating Eq. (11) in the presence of excess imprecision $\bar{S}_{xx}^{\rm imp,cl}$, as compared to $\bar{n}_{\rm min}^{\rm fb} \approx 15$ were $\bar{S}_{xx}^{\rm imp,cl}$ negligible [see Fig. 4(b)]. Two possible causes of excess noise include cooling beam bleedthrough to the probe homodyne spectrum, due to imperfect polarization control, and residual TIN. However, other sources cannot be ruled out based on an extended analysis discussed in Supplement 1.

5. DISCUSSION

Regarding improvements to the experiment's performance, first and foremost, better alignment should help remedy the most significant optical losses due to poor mode matching between the cavity mode and the single-mode fiber. This should be possible by using a more precise alignment stage that positions the fiber with the fiber mirror before gluing it in place and, in particular, sets the pitch and yaw angles relative to the exoskeleton mirror. Namely, while the maximally attainable mode-matching efficiency is determined by the decentration of the fiber mirror vertex with respect to the fiber core, efficiencies of the order of 80% have been achieved with fiber cavities [48], an ∼20-fold improvement over the current performance. Improved mode matching would simultaneously allow higher intracavity powers, even with the rest of the experiment unchanged, so that $C_{\rm q} \sim 2$ can be reached and combined with homodyne detection. It would also mitigate two

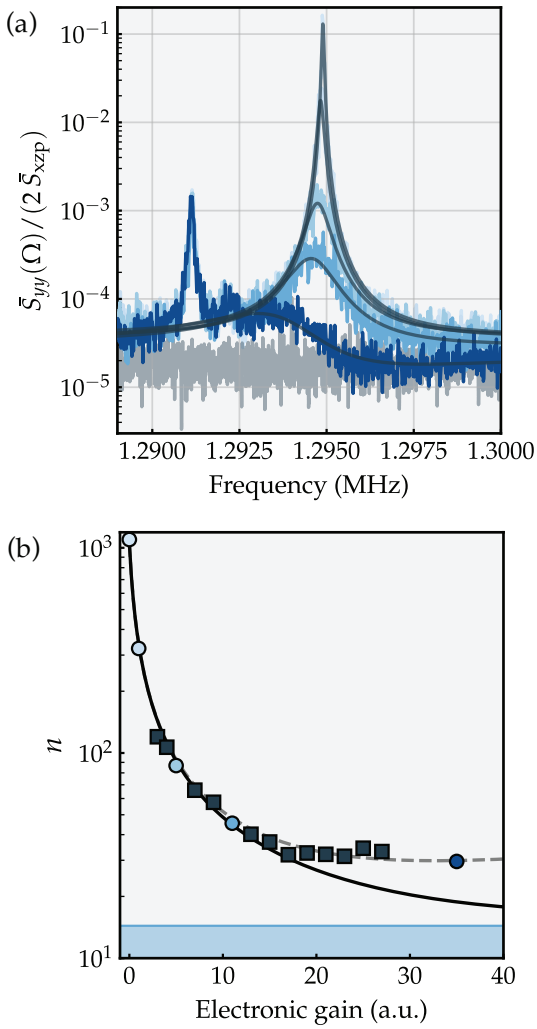

Fig. 4. (a) Measured mechanical spectra for progressively higher feedback gains from light to dark blue. The lightest trace is obtained with pure sideband cooling and is used as a calibration anchor. The right peak is the mode of interest, corresponding to the higher-frequency defect mode in Fig. 1(c), now shifted by the optical spring. The gray trace corresponds to shot noise of the light. Dark gray lines are fits to the data. The feature to the left is a stiff mechanical mode not susceptible to radiation pressure effects, and is excluded from the fit. (b) Occupation inferred from fits to the sideband- and feedback-cooled spectra as a function of electronic gain. Circles are color coded to the corresponding traces in (a), whereas squares correspond to data not shown in (a) for clarity. The solid black line is the theoretical prediction for quantum-limited imprecision (cf. Supplement 1), whereas the dashed gray line includes excess noise. The top of the blue-shaded region indicates the ideal-filter threshold, $\bar{n}_{\mathrm{min}}^{\mathrm{fb}}$.

of the potential contributions to classical imprecision, which stem from imperfect control of the cooling beam polarization (by allowing for a larger LO power) and from TIN (by enabling stronger sideband cooling). In the absence of other imprecision noise, realistic further improvements to an overall detection efficiency of $\eta_{\mathrm{det}} = 50\%$ then enable $\bar{n} < 1$ even in the presence of fiber mirror noise, according to Eq. (7). To reach $\bar{n} < 0.5$, the mirror noise could be suppressed by a factor of 10. This might be accomplished by replacing the fiber mirror with a second exoskeleton mirror, featuring a concave indentation made by laser ablation [72] or by solvent vapor reflow and reactive ion etching [73].

In comparison with other experiments performing feedback cooling of room-temperature devices, our achieved occupancy is orders of magnitude below what has been demonstrated with most suspended mechanical systems [53,74,75] and on par with state-of-the-art nanodevices ($\bar{n} = 27$) [41], as well as the test masses in advanced LIGO ($\bar{n} = 11$) [45]. Lower occupancies ($\bar{n} < 1$) have recently been achieved with nanoparticles held in optical traps [39,40], which are some five orders of magnitude lighter than the resonators studied here. We see a great potential of the membrane platform for room-temperature quantum experiments, due to its relative simplicity and great versatility. In addition to the many possibilities arising from a quantum-enabled optomechanical interface (see Introduction), membrane resonators can be functionalized to couple to charge [23,24] or spin [27,28], and can be decorated with samples such as viruses or metal nanoparticles [30]. This opens many application prospects that may benefit from initializing the mechanical system in a low-entropy state, e.g., by allowing to discern small displacements in phase space. A particularly interesting prospect would also be to implement a compact, wavelength-agnostic, room-temperature source of broadband ponderomotive squeezing [76].

Funding. H2020 Marie Skłodowska-Curie Actions (722923); Schweizerischer Nationalfonds zur Förderung der Wissenschaftlichen Forschung (177198); Novo Nordisk Fonden (NNF20OC0061866); Natur og Univers, Det Frie Forskningsråd (1026-00345B); Danmarks Grundforskningsfond (Hy-Q); European Research Council (101002179, 638765).

Acknowledgment. The authors thank David Hunger of Karlsruhe Institut für Technologie for access to and training on their setup for fabricating and characterizing fiber mirrors. The authors also thank Eva Weig of Technische Universität München for equipment and help in preparing the fibers and Irene Sánchez Arribas for assisting in fiber fabrication. Finally, the authors acknowledge Rik van Herk for acquiring and analyzing the data for the mechanical quality factor as a function of pressure, shown in Supplement 1.

Disclosures. The authors declare no conflicts of interest.

Data availability. Processed data corresponding to the figures in the main text are available in the Zenodo open repository [77], together with a Jupyter notebook to plot the figures. The underlying raw data may be obtained from the corresponding author upon reasonable request.

Supplemental document. See Supplement 1 for supporting content.

[†]These authors contributed equally to this work.

REFERENCES

1. J. D. Thompson, B. M. Zwickl, A. M. Jayich, F. Marquardt, S. M. Girvin, and J. G. E. Harris, "Strong dispersive coupling of a high finesse cavity to a micromechanical membrane," Nature **452**, 72–75 (2008).
2. D. J. Wilson, C. A. Regal, S. B. Papp, and H. J. Kimble, "Cavity optomechanics with stoichiometric sin films," Phys. Rev. Lett. **103**, 207204 (2009).
3. A. M. Jayich, J. C. Sankey, K. Bjorkje, D. Lee, C. Yang, M. Underwood, L. Childress, A. Petrenko, S. M. Girvin, and J. G. E. Harris, "Cryogenic optomechanics with a Si_3N_4 membrane and classical laser noise," New J. Phys. **14**, 115018 (2012).
4. N. E. Flowers-Jacobs, S. W. Hoch, J. C. Sankey, A. Kashkanova, A. M. Jayich, C. Deutsch, J. Reichel, and J. G. E. Harris, "Fiber-cavity-based optomechanical device," Appl. Phys. Lett. **101**, 221109 (2012).
5. F. Rochau, I. Sánchez Arribas, A. Brieussel, S. Stapfner, D. Hunger, and E. M. Weig, "Dynamical backaction in an ultrahigh-finesse fiber-based microcavity," Phys. Rev. Appl. **16**, 014013 (2021).
6. T. P. Purdy, R. W. Peterson, and C. A. Regal, "Observation of radiation pressure shot noise on a macroscopic object," Science **339**, 801–804 (2013).
7. M. Karuza, C. Biancofiore, M. Bawaj, C. Molinelli, M. Galassi, R. Natali, P. Tombesi, G. Di Giuseppe, and D. Vitali, "Optomechanically induced transparency in a membrane-in-the-middle setup at room temperature," Phys. Rev. A **88**, 013804 (2013).

8. T. P. Purdy, P.-L. Yu, N. S. Kampel, R. W. Peterson, K. Cicak, R. W. Simmonds, and C. A. Regal, "Optomechanical Raman-ratio thermometry," Phys. Rev. A **92**, 031802 (2015).
9. I. Galinskiy, Y. Tsaturyan, M. Parniak, and E. S. Polzik, "Phonon counting thermometry of an ultracoherent membrane resonator near its motional ground state," Optica **7**, 718–725 (2020).
10. C. B. Møller, R. A. Thomas, G. Vasilakis, E. Zeuthen, Y. Tsaturyan, M. Balabas, K. Jensen, A. Schliesser, K. Hammerer, and E. S. Polzik, "Quantum back-action-evading measurement of motion in a negative mass reference frame," Nature **547**, 191–195 (2017).
11. P. Christoph, T. Wagner, H. Zhong, R. Wiesendanger, K. Sengstock, A. Schwarz, and C. Becker, "Combined feedback and sympathetic cooling of a mechanical oscillator coupled to ultracold atoms," New J. Phys. **20**, 093020 (2018).
12. T. M. Karg, B. Gouraud, C. T. Ngai, G.-L. Schmid, K. Hammerer, and P. Treutlein, "Light-mediated strong coupling between a mechanical oscillator and atomic spins 1 meter apart," Science **369**, 174–179 (2020).
13. R. A. Thomas, M. Parniak, C. østfeldt, C. B. Møller, C. Bærentsen, Y. Tsaturyan, A. Schliesser, J. Appel, E. Zeuthen, and E. S. Polzik, "Entanglement between distant macroscopic mechanical and spin systems," Nat. Phys. **17**, 228–233 (2021).
14. Y. Ma, S. L. Danilishin, C. Zhao, H. Miao, W. Z. Korth, Y. Chen, R. L. Ward, and D. Blair, "Narrowing the filter-cavity bandwidth in gravitational-wave detectors via optomechanical interaction," Phys. Rev. Lett. **113**, 151102 (2014).
15. J. Qin, C. Zhao, Y. Ma, X. Chen, L. Ju, and D. G. Blair, "Classical demonstration of frequency-dependent noise ellipse rotation using optomechanically induced transparency," Phys. Rev. A **89**, 041802 (2014).
16. M. A. Page, M. Goryachev, H. Miao, Y. Chen, Y. Ma, D. Mason, M. Rossi, C. D. Blair, L. Ju, D. G. Blair, A. Schliesser, M. E. Tobar, and C. Zhao, "Gravitational wave detectors with broadband high frequency sensitivity," Commun. Phys. **4**, 1–8 (2021).
17. A. B. Shkarin, N. E. Flowers-Jacobs, S. W. Hoch, A. D. Kashkanova, C. Deutsch, J. Reichel, and J. G. E. Harris, "Optically mediated hybridization between two mechanical modes," Phys. Rev. Lett. **112**, 013602 (2014).
18. W. H. P. Nielsen, Y. Tsaturyan, C. B. Møller, E. S. Polzik, and A. Schliesser, "Multimode optomechanical system in the quantum regime," Proc. Natl. Acad. Sci. USA **144**, 62–66 (2017).
19. V. Fedoseev, F. Luna, I. Hedgepeth, W. Löffler, and D. Bouwmeester, "Stimulated Raman adiabatic passage in optomechanics," Phys. Rev. Lett. **126**, 113601 (2021).
20. H. Xu, D. Mason, L. Jiang, and J. G. E. Harris, "Topological energy transfer in an optomechanical system with exceptional points," Nature **537**, 80–83 (2016).
21. T. P. Purdy, P.-L. Yu, R. W. Peterson, N. S. Kampel, and C. A. Regal, "Strong optomechanical squeezing of light," Phys. Rev. X **3**, 031012 (2013).
22. J. Chen, M. Rossi, D. Mason, and A. Schliesser, "Entanglement of propagating optical modes via a mechanical interface," Nat. Commun. **11**, 1–6 (2020).
23. T. Bagci, A. Simonsen, S. Schmid, L. G. Villanueva, E. Zeuthen, J. Appel, J. M. Taylor, A. Sørensen, K. Usami, A. Schliesser, and E. S. Polzik, "Optical detection of radio waves through a nanomechanical transducer," Nature **507**, 81 (2014).
24. R. W. Andrews, R. W. Peterson, T. P. Purdy, K. Cicak, R. W. Simmonds, C. A. Regal, and K. W. Lehnert, "Reversible and efficient conversion between microwave and optical light," Nat. Phys. **10**, 321 (2014).
25. A. P. Higginbotham, P. S. Burns, M. D. Urmey, R. W. Peterson, N. S. Kampel, B. M. Brubaker, G. Smith, K. W. Lehnert, and C. A. Regal, "Harnessing electro-optic correlations in an efficient mechanical converter," Nat. Phys. **14**, 1038–1042 (2018).
26. B. M. Brubaker, J. M. Kindem, M. D. Urmey, S. Mittal, R. D. Delaney, P. S. Burns, M. R. Vissers, K. W. Lehnert, and C. A. Regal, "Optomechanical ground-state cooling in a continuous and efficient electro-optic transducer," Phys. Rev. X **12**, 021062 (2021).
27. R. Fischer, D. P. McNally, C. Reetz, G. G. T. Assumpção, T. Knief, Y. Lin, and C. A. Regal, "Spin detection with a micromechanical trampoline: towards magnetic resonance microscopy harnessing cavity optomechanics," New J. Phys. **21**, 043049 (2019).
28. J. Košata, O. Zilberberg, C. L. Degen, R. Chitra, and A. Eichler, "Spin detection via parametric frequency conversion in a membrane resonator," Phys. Rev. Appl. **14**, 014042 (2020).
29. L. Catalini, Y. Tsaturyan, and A. Schliesser, "Soft-clamped phononic dimers for mechanical sensing and transduction," Phys. Rev. Appl. **14**, 014041 (2020).
30. D. Hälg, T. Gisler, Y. Tsaturyan, L. Catalini, U. Grob, M.-D. Krass, M. Héritier, H. Mattiat, A.-K. Thamm, R. Schirhagl, E. C. Langman, A. Schliesser, C. L. Degen, and A. Eichler, "Membrane-based scanning force microscopy," Phys. Rev. Appl. **15**, L021001 (2021).
31. C. Reinhardt, T. Müller, A. Bourassa, and J. C. Sankey, "Ultralow-noise sin trampoline resonators for sensing and optomechanics," Phys. Rev. X **6**, 021001 (2016).
32. R. Norte, J. P. Moura, and S. Gröblacher, "Mechanical resonators for quantum optomechanics experiments at room temperature," Phys. Rev. Lett. **116**, 147202 (2016).
33. Y. Tsaturyan, A. Barg, E. S. Polzik, and A. Schliesser, "Ultracoherent nanomechanical resonators via soft clamping and dissipation dilution," Nat. Nanotechnol. **12**, 776–783 (2017).
34. M. Rossi, D. Mason, J. Chen, Y. Tsaturyan, and A. Schliesser, "Measurement-based quantum control of mechanical motion," Nature **563**, 53–58 (2018).
35. M. Rossi, D. Mason, J. Chen, and A. Schliesser, "Observing and verifying the quantum trajectory of a mechanical resonator," Phys. Rev. Lett. **123**, 163601 (2019).
36. S. P. Vyatchanin and E. A. Zubova, "Quantum variation measurement of a force," Phys. Lett. A **201**, 269–274 (1995).
37. N. S. Kampel, R. W. Peterson, R. Fischer, P.-L. Yu, K. Cicak, R. W. Simmonds, K. W. Lehnert, and C. A. Regal, "Improving broadband displacement detection with quantum correlations," Phys. Rev. X **7**, 021008 (2017).
38. D. Mason, J. Chen, M. Rossi, Y. Tsaturyan, and A. Schliesser, "Continuous force and displacement measurement below the standard quantum limit," Nat. Phys. **15**, 745–749 (2019).
39. U. Delic, M. Reisenbauer, K. Dare, D. Grass, V. Vuletic, N. Kiesel, and M. Aspelmeyer, "Cooling of a levitated nanoparticle to the motional quantum ground state," Science **367**, 892–895 (2020).
40. L. Magrini, P. Rosenzweig, C. Bach, A. Deutschmann-Olek, S. G. Hofer, S. Hong, N. Kiesel, A. Kugi, and M. Aspelmeyer, "Real-time optimal quantum control of mechanical motion at room temperature," Nature **595**, 373–377 (2021).
41. J. Guo, R. Norte, and S. Gröblacher, "Feedback cooling of a room temperature mechanical oscillator close to its motional ground state," Phys. Rev. Lett. **123**, 223602 (2019).
42. V. Sudhir, R. Schilling, S. Fedorov, H. Schütz, D. Wilson, and T. Kippenberg, "Quantum correlations of light from a room-temperature mechanical oscillator," Phys. Rev. X **7**, 031055 (2017).
43. T. P. Purdy, K. E. Grutter, K. Srinivasan, and J. M. Taylor, "Quantum correlations from a room-temperature optomechanical cavity," Science **356**, 1265–1268 (2017).
44. J. Cripe, N. Aggarwal, R. Lanza, A. Libson, R. Singh, P. Heu, D. Follman, G. D. Cole, N. Mavalvala, and T. Corbitt, "Measurement of quantum back action in the audio band at room temperature," Nature **568**, 364–367 (2019).
45. C. Whittle, E. D. Hall, S. Dwyer, *et al.*, "Approaching the motional ground state of a 10-kg object," Science **372**, 1333–1336 (2021).
46. M. Aspelmeyer, T. J. Kippenberg, and F. Marquardt, "Cavity optomechanics," Rev. Mod. Phys. **86**, 1391–1452 (2014).
47. W. P. Bowen and G. J. Milburn, *Quantum Optomechanics* (Taylor & Francis, 2016).
48. D. Hunger, T. Steinmetz, Y. Colombe, C. Deutsch, T. W. Hänsch, and J. Reichel, "A fiber Fabry–Perot cavity with high finesse," New J. Phys. **12**, 065038 (2010).
49. D. Hunger, C. Deutsch, R. J. Barbour, R. J. Warburton, and J. Reichel, "Laser micro-fabrication of concave, low-roughness features in silica," AIP Adv. **2**, 012119 (2012).
50. J. Gallego, S. Ghosh, S. K. Alavi, W. Alt, M. Martinez-Dorantes, D. Meschede, and L. Ratschbacher, "High-finesse fiber Fabry–Perot cavities: stabilization and mode matching analysis," Appl. Phys. B **122**, 47 (2016).
51. S. Mancini, D. Vitali, and P. Tombesi, "Optomechanical cooling of a macroscopic oscillator by homodyne feedback," Phys. Rev. Lett. **80**, 688–691 (1998).
52. P.-F. Cohadon, A. Heidmann, and M. Pinard, "Cooling of a mirror by radiation pressure," Phys. Rev. Lett. **83**, 3174–3177 (1999).
53. D. Kleckner and D. Bouwmeester, "Sub-kelvin optical cooling of a micromechanical resonator," Nature **444**, 75–78 (2006).

54. D. J. Wilson, V. Sudhir, N. Piro, R. Schilling, A. Ghadimi, and T. J. Kippenberg, "Measurement-based control of a mechanical oscillator at its thermal decoherence rate," Nature **524**, 325–329 (2015).
55. V. B. Braginsky and F. Y. Khalili, *Quantum Measurement* (Cambridge University, 1992).
56. A. Schliesser and T. J. Kippenberg, *Cavity Optomechanics with Whispering-Gallery-Mode Optical Microresonators* (Elsevier/Academic, 2010), Vol. **58**, pp. 207–323.
57. A. Schliesser, R. Rivière, G. Anetsberger, O. Arcizet, and T. Kippenberg, "Resolved-sideband cooling of a micromechanical oscillator," Nat. Phys. **4**, 415–419 (2008).
58. P. Rabl, C. Genes, K. Hammerer, and M. Aspelmeyer, "Phase-noise induced limitations in resolved-sideband cavity cooling of mechanical resonators," Phys. Rev. A **80**, 063819 (2009).
59. A. H. Safavi-Naeini, J. Chan, J. T. Hill, S. Gröblacher, H. Miao, Y. Chen, M. Aspelmeyer, and O. Painter, "Laser noise in cavity-optomechanical cooling and thermometry," New J. Phys. **15**, 035007 (2013).
60. NKT photonics (personal communication, 2022).
61. S. A. Fedorov, A. Beccari, A. Arabmoheghi, D. J. Wilson, N. J. Engelsen, and T. J. Kippenberg, "Thermal intermodulation noise in cavity-based measurements," Optica **7**, 1609–1616 (2020).
62. M. Rossi, "Quantum measurement and control of a mechanical resonator," Ph.D. thesis (University of Copenhagen, 2020).
63. V. B. Braginsky, M. L. Gorodetsky, and S. P. Vyatchanin, *Compendium of Thermal Noises in Optical Mirrors* (Cambridge University, 2012), pp. 20–30.
64. T. Briant, P.-F. Cohadon, A. Heidmann, and M. Pinard, "Optomechanical characterization of acoustic modes in a mirror," Phys. Rev. A **68**, 033823 (2003).
65. D. J. Wilson, "Cavity optomechanics with high-stress silicon nitride films," Ph.D. thesis (California Institute of Technology, 2012).
66. W. H. P. Nielsen, "Quantum cavity optomechanics with phononic bandgap shielded silicon nitride membranes," Ph.D. thesis (University of Copenhagen, 2016).
67. T. P. Purdy, R. W. Peterson, P.-L. Yu, and C. A. Regal, "Cavity optomechanics with Si_3N_4 membranes at cryogenic temperatures," New J. Phys. **14**, 115021 (2012).
68. Y. Tsaturyan, A. Barg, A. Simonsen, L. G. Villanueva, S. Schmid, A. Schliesser, and E. S. Polzik, "Demonstration of suppressed phonon tunneling losses in phononic bandgap shielded membrane resonators for high-Q optomechanics," Opt. Express **6**, 6810 (2013).
69. P.-L. Yu, K. Cicak, N. S. Kampel, Y. Tsaturyan, T. P. Purdy, R. W. Simmonds, and C. A. Regal, "A phononic bandgap shield for high-Q membrane microresonators," Appl. Phys. Lett. **104**, 023510 (2014).
70. R. M. Shelby, M. D. Levenson, and P. W. Bayer, "Guided acoustic-wave Brillouin scattering," Phys. Rev. B **31**, 5244–5252 (1985).
71. J. F. S. Brachmann, H. Kaupp, T. W. Hänsch, and D. Hunger, "Photothermal effects in ultra-precisely stabilized tunable microcavities," Opt. Express **24**, 21205–21215 (2016).
72. A. G. Kuhn, J. Teissier, L. Neuhaus, S. Zerkani, E. van Brackel, S. Deleglise, T. Briant, P.-F. Cohadon, A. Heidmann, C. Michel, L. Pinard, V. Dolique, R. Flaminio, R. Taïbi, C. Chartier, and O. Le Traon, "Free-space cavity optomechanics in a cryogenic environment," Appl. Phys. Lett. **104**, 044102 (2014).
73. N. Jin, C. A. McLemore, D. Mason, J. P. Hendrie, Y. Luo, M. L. Kelleher, P. Kharel, F. Quinlan, S. A. Diddams, and P. T. Rakich, "Micro-fabricated mirrors with finesse exceeding one million," Optica **9**, 965–970 (2022).
74. C. Schäfermeier, H. Kerdoncuff, U. B. Hoff, H. Fu, A. Huck, J. Bilek, G. I. Harris, W. P. Bowen, T. Gehring, and U. L. Andersen, "Quantum enhanced feedback cooling of a mechanical oscillator using nonclassical light," Nat. Commun. **7**, 13628 (2016).
75. C. M. Pluchar, A. R. Agrawal, E. Schenk, and D. J. Wilson, "Towards cavity-free ground-state cooling of an acoustic-frequency silicon nitride membrane," Appl. Opt. **59**, G107–G111 (2020).
76. N. Aggarwal, T. J. Cullen, J. Cripe, G. D. Cole, R. Lanza, A. Libson, D. Follman, P. Heu, T. Corbitt, and N. Mavalvala, "Room-temperature optomechanical squeezing," Nat. Phys. **16**, 784–788 (2020).
77. S. A. Saarinen, N. Kralj, E. C. Langman, Y. Tsaturyan, and A. Schliesser, "Laser cooling a membrane-in-the-middle system close to the quantum ground state from room temperature," Zenodo, 2023, https://doi.org/10.5281/zenodo.7647319.